actuators

MDPI

Article

A Soft Electro-Hydraulic Pneumatic Actuator with Self-Sensing Capability toward Multi-Modal Haptic Feedback

Haoyu Wang [1,2,†], Xiang Cheng [2,†], Pei Huang [2,3], Meng Yu [2,4], Jiaqi Ma [1], Shigang Peng [2], Yue Cheng [1], Yuan Yu [1], Weimin Yang [1], Pengfei Wang [2,*] and Zhiwei Jiao [1,*]

1 College of Mechanical and Electrical Engineering, Beijing University of Chemical Technology, Beijing 100029, China; hywang22@buct.edu.cn (H.W.); majiaqi@bzkj.cn (J.M.); 2021400183@buct.edu.cn (Y.C.); yuyuan@mail.buct.edu.cn (Y.Y.); yangwm@mail.buct.edu.cn (W.Y.)
2 Qian Xuesen Laboratory of Space Technology, China Academy of Space Technology, Beijing 100094, China; chengxiang@qxslab.cn (X.C.); huangpei@emails.bjut.edu.cn (P.H.); yvmeng1994@gmail.com (M.Y.); luyueyangguang@163.com (S.P.)
3 School of Energy and Power Engineering, Nanjing University of Science and Technology, Nanjing 210094, China
4 School of Aerospace Engineering, Beijing Institute of Technology, Beijing 100081, China
* Correspondence: wangpengfei@qxslab.cn (P.W.); jiaozw@mail.buct.edu.cn (Z.J.)
† These authors contributed equally to this work.

Abstract: Haptic feedback is appealing for achieving the realistic perception of environmental changes for human bodies in human–computer interaction fields. However, existing haptic actuators have some hurdles such as single mode, poor compatibility, or incomplete tactile information. In this study, we proposed a novel way to generate haptic feedback by designing a soft electro-hydraulic pneumatic actuator (SEHPA) with dual drive modes. The SEHPA was structured with silicone films, a silicone air chamber, flexible electrodes, and an insulating liquid dielectric for good human–machine compatibility. The SEHPA had the advantages of high output force (1.5 N at 10 kPa) and displacement (4.5 mm at 5 kPa), as well as various haptic notifications (0~400 Hz vibration). The electro-hydraulic drive method realized smooth output force changes at the millinewton level (0~40 mN) and output displacement changes at the micron level (0~800 μm), which further enriched the details of the tactile experience. In addition, the self-sensing capability of the SEHPA can be dedicated to monitoring and ensuring precise output. The SEHPAs can be potentially mounted on the fingertips to provide accurate tactile sensation once the manipulator touches an object through teleoperation. More invisible information can also be obtained by customizing various haptic notifications. The excellent response behavior and accurate tactile haptic feedback demonstrate the candidate for teleoperation fields.

Keywords: soft electro-hydraulic pneumatic actuator; self-sensing; haptic feedback; haptic notifications

Citation: Wang, H.; Cheng, X.; Huang, P.; Yu, M.; Ma, J.; Peng, S.; Cheng, Y.; Yu, Y.; Yang, W.; Wang, P.; et al. A Soft Electro-Hydraulic Pneumatic Actuator with Self-Sensing Capability toward Multi-Modal Haptic Feedback. *Actuators* **2022**, *11*, 74. https://doi.org/10.3390/act11030074

Academic Editor: Giorgio Olmi

Received: 25 January 2022
Accepted: 28 February 2022
Published: 2 March 2022

1. Introduction

Tactile sensation plays a very important role in feeling subtle changes in the environment. In virtual reality and augmented reality, a full, immersive experience not only includes interactive images and sounds, but also involves the sensations of touch [1]. In the field of human–computer interaction and teleoperation, tactile sensation can help the operator to regulate behavior and give hints to the upcoming danger, thereby increasing the safety of the operation. Therefore, a haptic feedback actuator is urgently needed to simulate and reproduce human touch. Feedback actuators are expected to exhibit the characteristics of safety, rapid response, rich tactility, etc., which can remind people of the tactility quickly and perfectly.

Traditional rigid haptic feedback devices have generally adopted rigid mechanical devices such as motors, electromagnets, and hydraulic mechanisms [2,3], which would be hindered by their complex structures and large volumes. The latest miniaturized drive

devices can apply vibration [4] to the fingertips or use needle-like arrays [5] and small mobile platforms [6] to provide passive haptic feedback in the contact area. The emergence of smart soft materials has allowed the flexible micro-drive structure to arbitrarily change its shape and size according to actual needs, as well as strong impact resistance and good environmental compatibility. Smart soft materials and structures play an important role in the design and practical application of flexible micro-drive structures, and their special drive mechanism greatly expands the functions of flexible micro-drive structures [7–14].

According to the driving modes, the existing soft haptic actuators can be categorized into pneumatic drives, electro-hydraulic drives, electromagnetic drives, and so on. Lee et al. [15] designed a three-axis pneumatic haptic actuator, where the device provided a lateral displacement of $\pm$1.5 mm for shear haptic feedback and a vertical inflation of the balloon of up to 3.7 mm for normal haptic feedback. Li et al. [16] proposed a multi-fingered palpation method, in which the employed pneumatic haptic feedback actuators, with the produced displacements of 4.5 mm at 100 kPa, allowed users to experience haptic sensations at multiple fingers while carrying out remote soft tissue palpation. Song et al. [17] designed a pneumatic haptic feedback actuator for virtual VR systems. The electrostatic attraction moved downward to the ring electrode, the air in the enclosed cavity then moved to the center, and the center area was thus raised, which generated the haptic feedback on the human finger. The maximum output displacement was about 0.13 mm. Uramune et al. [18] proposed a haptic display with a liquid-to-gas phase change actuator and Peltier device. The actuator was composed of a thin plastic pouch containing a low-boiling-point liquid. The maximum output force of the actuator could reach almost 1.5 N. Carpi et al. [19] reported a nonvibratory display of softness made of electroactive polymers. It consisted of a hydrostatically coupled dielectric elastomer actuator, shaped as a bubble interfaced to the fingertip, having a weight of 6 g. Prototypes could generate displacements up to 3.5 mm and forces up to 1 N. Leroy et al. [20] proposed multimode hydraulically amplified electrostatic actuators for wearable haptics. The 6 mm $\times$ 6 mm $\times$ 0.8 mm actuator weighed 90 mg, and generated forces of over 300 mN, out-of-plane displacements of 500 µm (over 60% strain), and lateral motion of 760 µm. Choi et al. [21] prepared silicone films and flexible electrodes by spin-coating and spraying methods to form an 8-layer 4 $\times$ 5 microarray structure with an overall thickness of about 210 µm. The unit applied a voltage of 3.5 kV to achieve a maximum displacement of 471 µm and a force-to-weight ratio of about 7 N/g. Ghosh et al. [22] prepared a silicone tube dielectric elastomer actuator. The response time of the 20 mm-length actuator was about 0.7 s, and the displacement reached 1 mm under a voltage of about 100 kV/mm. Yu et al. [1] presented a platform of electronic systems and haptic interfaces capable of softly laminating onto the curved surfaces of the skin to communicate information via spatiotemporally programmable patterns of localized mechanical vibrations. The output force of the device could reach 135 mN and the maximum displacement could reach 35 µm. In summary, pneumatic actuators can produce high output forces and displacements. Although pneumatic actuators have shown high-frequency switching with a few percent of strain change in closed-loop sensing, actuation, and control [23], the bandwidth here is limited due to the resistance of the tubing length and diameter compared to the possibility of actuation resolution, especially with the use of high-speed piezo-regulators [24]. Actuators driven by electric fields can provide higher resolutions, but it is difficult for the actuators to achieve high output forces while maintaining the corresponding high bandwidth. Actuators driven by magnetic fields can generate high-frequency vibration, but the internal magnets will affect the flexibility of the actuator. More importantly, most current haptic feedback actuators, without self-sensing capability, make the output unrepeatable and therefore cannot produce stable haptic feedback. This instability makes it impossible for people to perceive small tactile changes. Haptic feedback actuators have been widely studied, but their structure and the driven mode still need to be explored and designed to improve the output force and enrich the tactile sensation. The disadvantages of the single-drive approach are obvious; more complex tactic sensations could need to be expressed with the synergy of different drive modes.

In this paper, a SEHPA was proposed for haptic feedback. We carried out structural design and material selection for the SEHPA. All flexible units and their silicone material were adopted to imitate human skin [25], which could perfectly fit human fingertips to reduce foreign body sensations. The synergy of dual drive modes, the similar materials to the elasticity of human skin, and the design of the structure allowed the actuator to be easily driven. The pressure input only needed 5~10 kPa, which could be easily achieved by using a small linear motor to drive the piston, and the voltage input needed 3~5 kV, which could be generated with a small high-voltage module. The high output power of the SEHPA had a strong impact on human fingertips, and the variation in vibrations gives humans richer haptic notifications [26]. The working status of the SEHPA could be monitored in real-time through the changes in its self-sensing resistance. The precision and stability of output force could be improved by closed-loop control. In addition, the SEHPA was capable of withstanding high voltages while generating large strains due to the hydraulically amplified and self-healing ability [27–29]. The SEHPA could increase human's tactile experience and is very suitable for flexible wearable devices.

2. Design

The SEHPA is made of an electro-hydraulic structure and an air chamber. The electro-hydraulic structure of the SEHPA is composed of multi-layer thin films, which are electrically driven to trigger the thickness change and produce variation. Meanwhile, the air chamber is installed below the electro-hydraulic structure, which is driven by air pressure to trigger the height change of the films. As shown in Figure 1, the parts of the SEHPA, from top to bottom, are silicone film, round flexible electrode, silicone film, insulating liquid dielectric, annular silicone film, silicone film, flexible electrode, silicone film, and silicone air cavity. The silicone layer is bonded by the same silicone matrix. The middle three layers of silicone are bonded to create a cavity, and the insulating liquid dielectric is injected into the cavity. The outer layers of silicone are used to seal the flexible electrode to ensure that people can touch it safely.

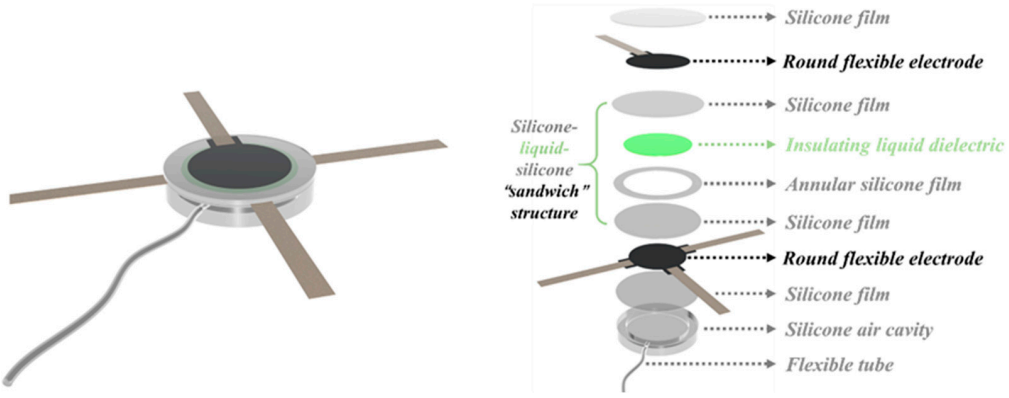

Figure 1. Exploded view of the SEHPA.

Figure 2a–c show the working principle of the SEHPA. When pressure is applied, the pressure is applied evenly on the flexible film, causing the film to deform and bulge upward. The liquid inside the film is redistributed to eliminate the internal stress in the direction perpendicular to the film and make the center part of the film more uniformly deformed. In this process, the stress along the direction of the film increases, providing powerful conditions for the voltage driving process. A Maxwell force occurs between the two circular electrodes when a voltage is applied, and the film is hence deformed, further increasing the area of the film. The film finally bulges upward due to the internal air pressure. In addition, the internal insulating liquid can not only transmit pressure, but also isolate the two electrodes, effectively increasing the breakdown voltage threshold of the actuator.

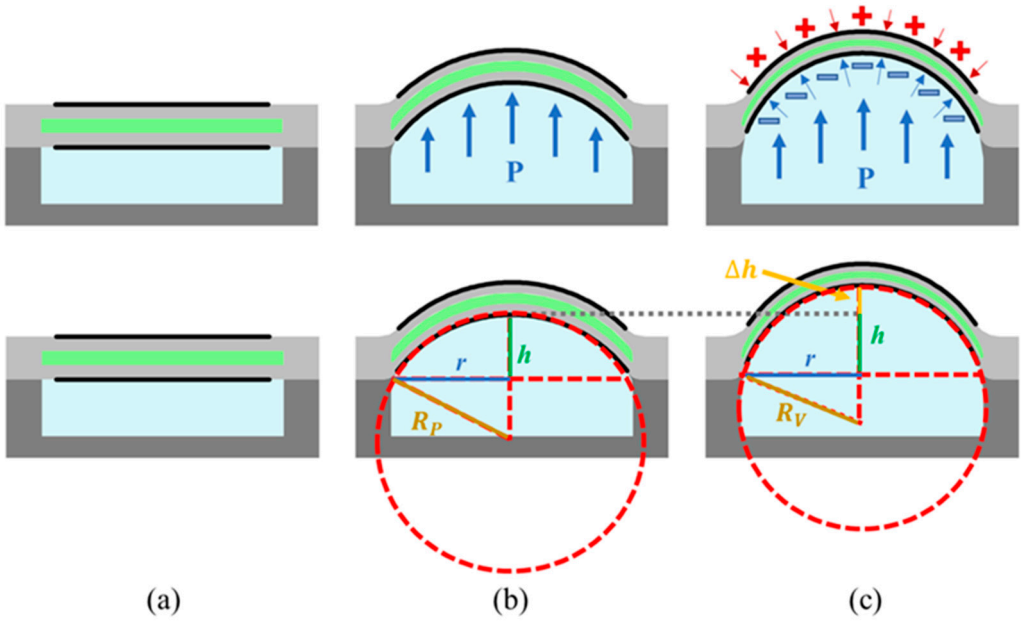

Figure 2. Schematic diagram of the SEHPA. (**a**) The initial state of the SEHPA. (**b**) Deformation driven by pressure. (**c**) Deformation driven by voltage.

The application of pressure and voltage will change the shape of the film, further affecting the output. The average strain of the film is correlated to the output displacement. Ignoring the slight change in the thickness of the film when it is deformed, the deformation state of the film after applying air pressure and voltage is shown in Figure 2b,c, respectively. The pressurized film will expand to be the curved surface of a spherical cap (defined by h, r, and R_P). R_P is the radius of the sphere and h is the displacement of the film. r is the inner radius of the air cavity, which is a constant value and will have a great influence on the output displacement h. On this basis, the applied voltage of the film is further deformed, R_P will change to R_V, and the change in height is Δh.

The area of the film before deformation is $S = \pi r^2$. The area of the curved surface of the spherical cap driven by pressure is $S_P = 2\pi rh$. The area of the curved spherical cap driven by voltage is $S_V = 2\pi r(h + \Delta h)$. The corresponding average strain of films is ε_P and ε_V.

$$\varepsilon_P = \frac{S_P}{S} = \frac{2h}{r} \left(h = \frac{\varepsilon_P \cdot r}{2}\right) \tag{1}$$

$$\varepsilon_V = \frac{S_V}{S_P} = \frac{h + \Delta h}{h} = 1 + \frac{2\Delta h}{\varepsilon_P r} \left(\Delta h = \frac{(\varepsilon V - 1) \cdot \varepsilon P \cdot r}{2}\right) \tag{2}$$

The deformation produced by the pneumatic drive can assist the electro-hydraulic drive to produce more obvious deformation. The size of r has a certain effect on the output displacement and strain. The larger the r, the more obvious the deformation, but it is more unfavorable for placing on fingertips. It is necessary to determine reasonable parameters through multiple experiments to obtain a good haptic feedback effect.

3. Materials and Methods

3.1. Fabrication

Figure 3 briefly describes the manufacturing process of the SEHPA. (A) Preparation of silicone film. Components A and B (ratio of 1:1) of liquid silicone (Ecoflex 00-30, Smooth-On, Macungie, PA, USA) were evenly mixed. Then, 4 mL of the liquid mixture was dripped onto an acrylic sheet covered with a BOPP film (BOPP Film, Kaida new packaging materials, Bazhou, China). The liquid silicone mixture was extruded into 2 round acrylic sheets with diameters of 113 mm. Then, the extruded mixture was cured at 25 °C for 6 h to obtain silicone films (thickness of 0.4 mm), where the coated BOPP film was favorable in the

further operation. (B) Laser cutting. The silicone film was cut into rings and circles by a laser cutting machine (VLS 3.50, Universal Laser Systems, Scottsdale, AZ, USA). The diameter of the circle was 20 mm. The outer diameter of the ring was 20 mm and the inner diameter was 7.5 mm. (C) Building a sandwich and injecting dielectric layer. The silicone films were bonded together, which is shown in Figure 3c. The FR3 insulating oil (Envirotemp FR3, Cargill, Wayzata, MN, USA) was injected into the cavity of the interzone and the air bubbles were drawn out of it. (D) Pre-stretching of the sandwich structure. The sandwich structure was pre-stretched, and the diameter was extended to 2 times that of the original. (E) Coating multiwalled carbon nanotube (MWCNT) electrodes. The upper and lower layers of the sandwich structure were evenly coated with MWCNTs (HQNANO-CNTs-010-0, Hengqiu graphene technology, Suzhou, China). The upper electrode was connected with 1 wire as the positive pole of the voltage applied. The lower electrode was connected with 3 wires, one of which was used as the negative pole of the voltage applied, and the other two wires served as the two signal channels of resistance detection. (F) Preparation of chamber. A 3D printer was used to make the cavity mold, and the gas pipe (outer diameter 1 mm, inner diameter 0.5 mm) was placed in the mold. Dragon Skin 30 silicone (Dragon Skin 30, Smooth-On) was used to make the cavity in the same way as before. (G) Demolding of silicone air cavity. The cavity was removed from the mold after being cured. (H) Integrating into the SEHPA. The SEHPA was successfully fabricated by integrating the sandwich structure with the flexible air chamber. Figure 3i shows the dimensions of the SEHPA. The flexibility of the SEHPA (Figure 3j) would assure its potential wearability.

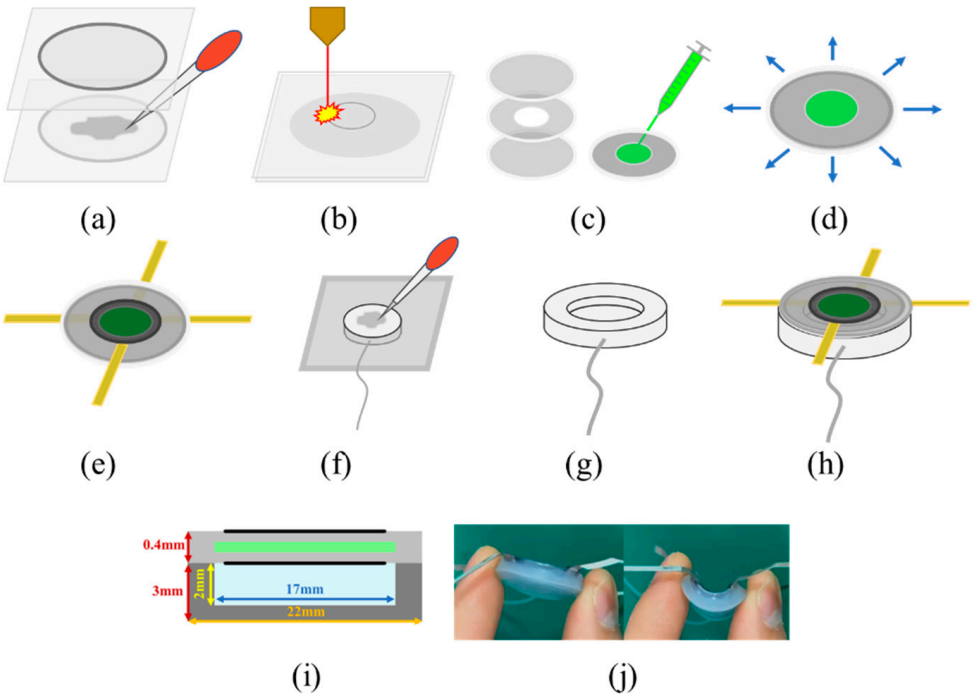

Figure 3. The preparation process of the SEHPA. (**a**) Preparation of silicone film. (**b**) Laser cutting. (**c**) Building a sandwich and injecting dielectric layer. (**d**) Pre-stretching of the sandwich structure. (**e**) Coating MWCNT electrodes. (**f**) Preparation of chamber. (**g**) Demolding of silicone air cavity. (**h**) Integration into SEHPA. (**i**) Size parameters of SEHPA. (**j**) Deformation of the SEHPA.

3.2. Test Methods

3.2.1. Output Displacement Measurement

Figure 4 shows the method for measuring the displacement of the SEHPA. The displacement of the center of the SEHPA was measured by a laser displacement sensor (HG-C1050, Panasonic, Osaka, Japan). Upon measurement, the gas pressure was generated

with a linear motor (LA16-021D, Inspire Robots, Beijing, China), and the DC voltages of 0–5 kV were loaded with a high-voltage module.

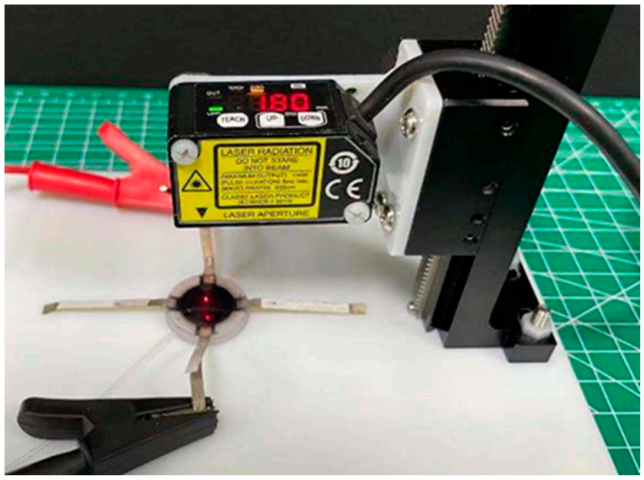

Figure 4. The output displacement measurement of the SEHPA.

3.2.2. Output Force Measurement

Figure 5 shows the output force measurement device of the SEHPA. The SEHPA was directly placed under the digital force gauge (HP-20, Handpi, Yueqing, China). The measuring head of the force gauge was wrapped with silicone material (Ecoflex 00-30, Smooth-On, Macungie, PA, USA), whose compressive behavior is comparable with that of human skin [25]. The curvature of the measuring head was also designed according to the curvature of the human finger. Therefore, this method could more accurately simulate the force of the finger and measure the output force.

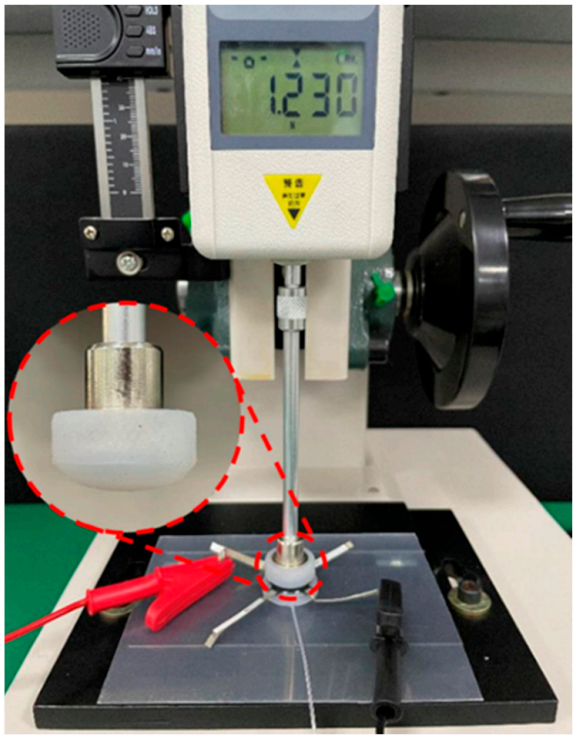

Figure 5. The output force measurement of the SEHPA. The inset is an enlarged view of the silicone wrapped test head.

3.2.3. Resistance Measurement

An LCR bridge (TH2830, Tonghui, Changzhou, China) was used to measure the resistance of the SEHPA. The LCR bridge was connected to a computer and test circuit to record the electrical signals, with a test time-interval of 0.1 s.

4. Results

4.1. Output Performance of SEHPA

4.1.1. Output Displacement of SEHPA

The output displacement of the SEHPA was characterized with the aforementioned method described in Section 3.2.1. The SEHPA output displacements under different pressures and voltage loadings are depicted in Figure 6. The output displacement curves, under all the six loaded voltages, were relatively proportional to the input pressure of 0.3~5 kPa, and the linear correlation was favorable. It was noticed that the six curves were coincident and flatter under the small input pressures of 0~0.3 kPa. The phenomenon can be interpreted with the two following reasons: (1) Under the pressures of 0~0.3 kPa, the silicone film was flat and thick, and the distance between the two electrodes was very far. The weak Maxwell force was not large enough to drive the film to deform. (2) The deformation mainly occurred at the lower film, and the internal liquid correspondingly flowed, therefore further making the output displacement unobvious. Moreover, the slopes of the curves increased with the applied voltages, which was owed to the higher Maxwell force at the voltage of 0.3~5 kPa.

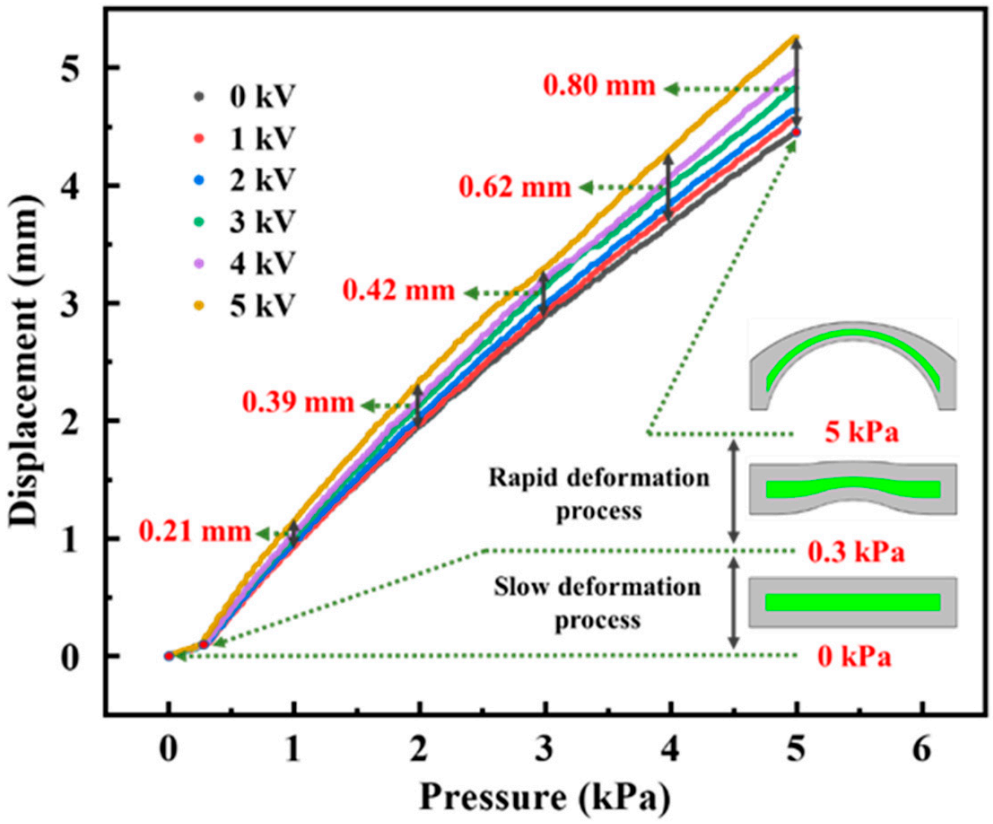

Figure 6. The output displacements of the SEHPA under different pressures and voltages.

The results also reveal that the applied voltage had a positive effect on the increment in the output displacements. For instance, the output displacement at 5 kV increased by 0.8 mm compared to that at 0 kV, at the pressure 5 kPa. Compared with the reported experimental results, the output displacement of the film could at least reach 5 mm, which is much larger than the reported displacement of some actuators [1,15–17,20,22].

4.1.2. Output Force of SEHPA

The generation of fingertip tactile sensations relies on a sensory organ that is referred to as the Merkel disc [30]. The Merkel disc is mainly concentrated on the fingertips, which has a high degree of tactile sensitivity and is very sensitive to skin pressure, hair movement, and other tactile stimuli. In this research, the output force of the SEHPA stimulating the Merkel disc was dedicated to simulating the hands' touch to objects. In order to measure the output force more accurately, we made a measuring indenter similar to the size, curvature, and elasticity of the fingertip. The effective radius and radius of curvature of the indenter were 7.5 mm and 19.5 mm, respectively. The material of the indenter was Ecoflex 00-30. The output force of the SEHPA was tested with the method described in Section 3.2.2. The SEHPA output forces under different pressures and voltage loadings are described in Figure 7. The curves between output force versus pressure were highly consistent, even under different voltages (0~5 kV). The effect of the pressure on the output force increment, under 5 kV, is shown in the inset. The output force increments seemed correlated with the pressure; namely, the increments were larger under higher pressure. The output force at 5 kV increased by 45 mN compared to that at 0 kV, under the condition of 8 kPa. The output force of the SEHPA could reach at least 1.5 N, which is larger than the reported force of the actuators [1,18,20,21].

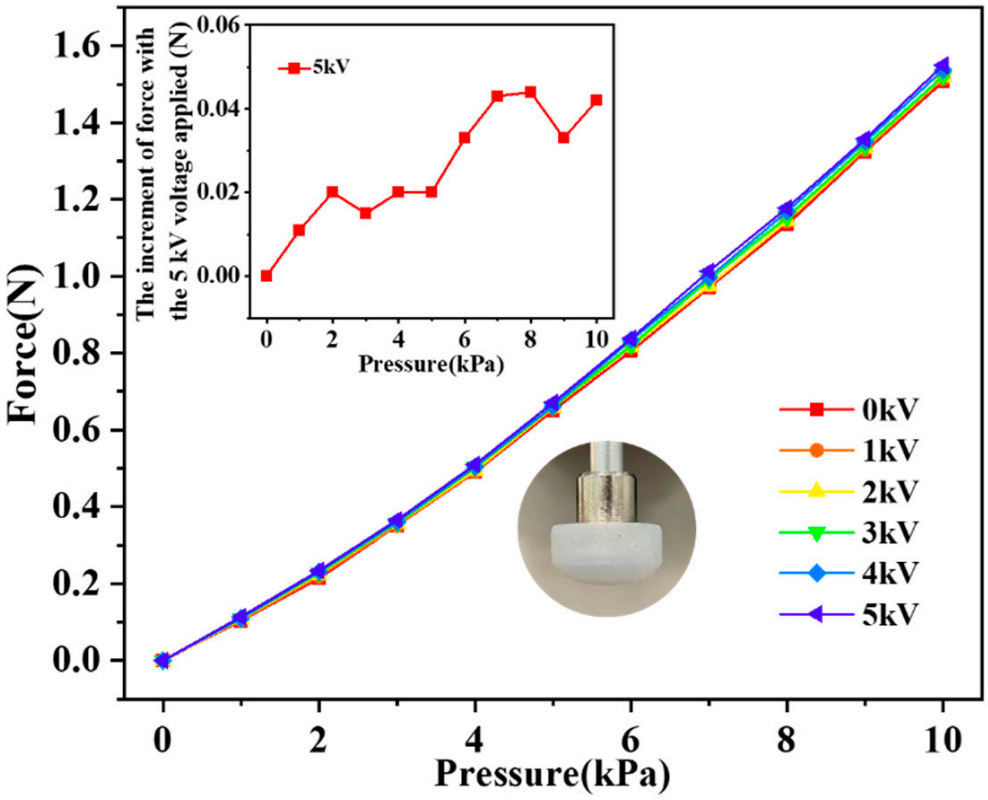

Figure 7. The output force of the SEHPA under different pressures and voltages. The inset shows the increment in the output force at 5 kV.

4.1.3. Self-Sensing Capability of SEHPA

The lower electrode of the SHEPA was chosen to test its resistance, as it was farther away from the fingertips and less affected by the external force; therefore, its resistance could better correspond to the deformed state of the SHEPA. The resistances of the lower electrode under various pressures are shown in Figures 8 and 9. The pressure was slowly applied, with a rate of 0.5 kPa/s, to guarantee the stable deformation of the SHEPA. It was found out the resistance increased with the loaded pressures, which was further related to the increases in the displacements and deformations of the lower electrode. The increase

in the area of the bulged film increased the distance between the neighboring MWCNTs, and the resistances hence increased [31,32]. The resistance of the lower electrode increased from the initial 59 kΩ to 238 kΩ when the pressure of 5 kPa was loaded. In the iso-pressure state (Figure 8), the resistance of the lower electrode slightly relaxed and then turned stable. Figure 9 shows the peak resistances (derived from Figure 8) and the corresponding deformation states of the SHEPA. It could be concluded that the resistance value of the lower electrode was well correlated to the displacement and output force. The output state of the SEHPA at different pressures is recorded in Video S1.

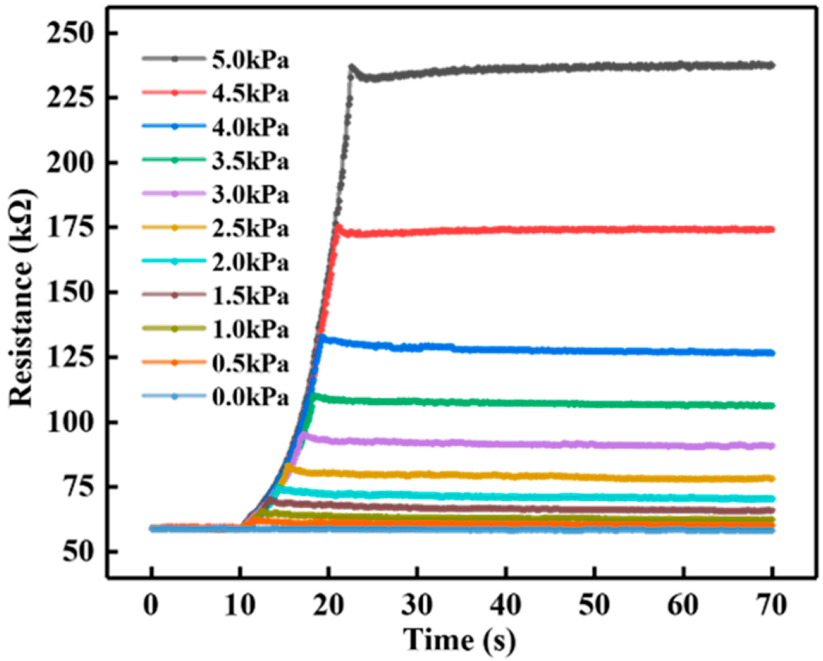

Figure 8. The resistance of the lower electrode of the SHEPA under different pressures, in which the pressurization rate is 0.5 kPa/s.

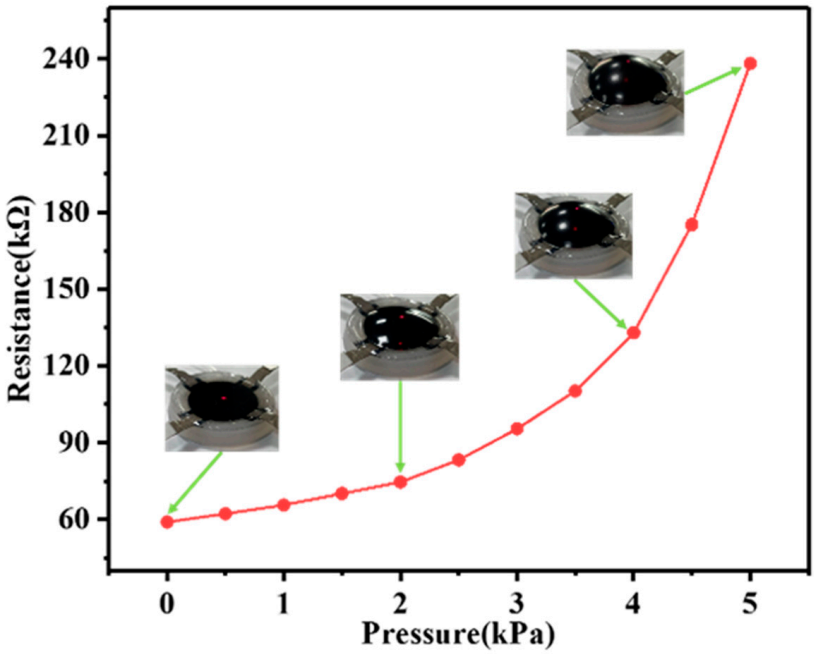

Figure 9. Peak resistances (derived from Figure 8) and the corresponding deformation states of SHEPA are shown in the insets.

4.1.4. The Response Time of SEHPA

The time needed for the SEHPA to deform to a stable state is thereby defined as the response time of the SEHPA, as described in Figure 10. In the measurements, the pressure of 5 kPa was quickly loaded and the time for the pressure to increase from 0 kPa to 5 kPa was about 0.27 s. The SEHPA simultaneously deformed once the pressure was loaded, and it still cost 0.23 s more to reach the maximum displacement after the 5 kPa was completely loaded. The voltage also influenced the final stable displacement. The displacement of the SEHPA reached a new equilibrium after a voltage of 5 kV was applied at about 7.34 s, and the response time cost for the SEHPA to the peak was about 0.08 s. The response time is an important parameter to an actuator to evaluate its response speed and the loading frequencies.

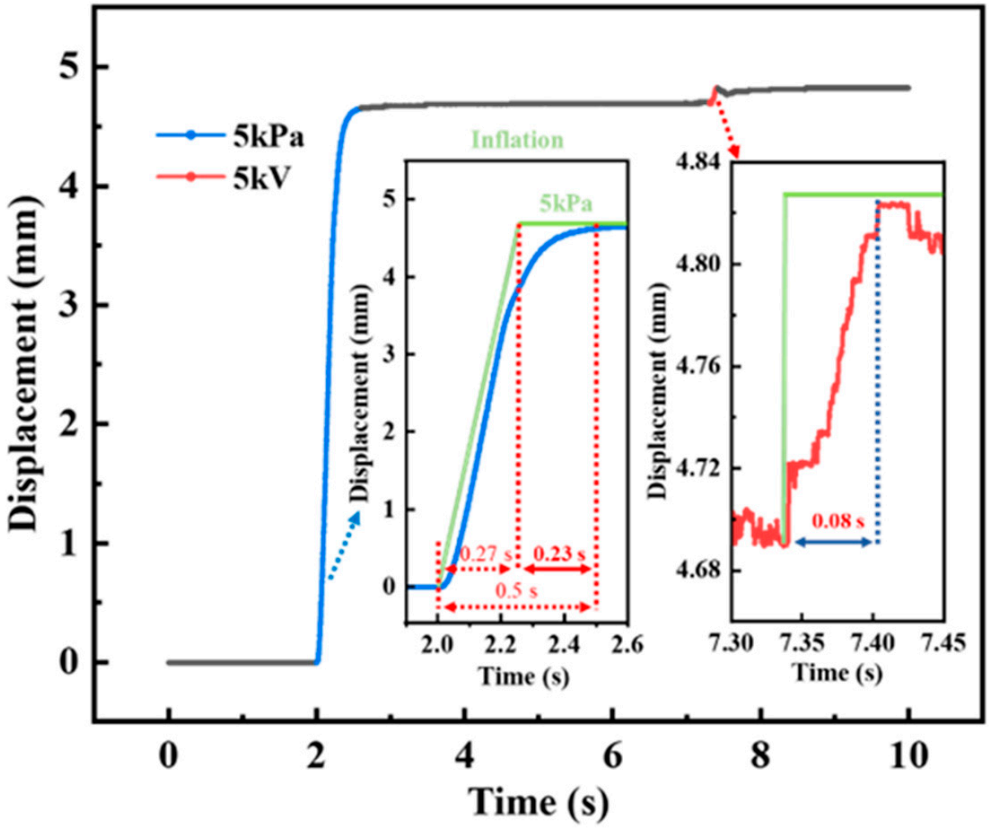

Figure 10. Response time of the SEHPA, in which 5 kPa was applied at 2 s and 5 kV was applied at about 7.34 s.

4.1.5. The Vibration of SEHPA

The displacements of the SEHPA, under the cyclic loading of 5 kV and with the loading frequencies of 0~400 Hz, are depicted in Figure 11. The test was to determine whether the SEHPA can produce displacement changes at these frequencies. The experimental results showed that the SEHPA could respond to displacement at voltage frequencies within 400 Hz. In the range from 0.5 Hz to 100 Hz (Figure 11a), the SEHPA vibrated, and the cyclic displacements decreased with the frequencies. This decrease in the cyclic displacements was owed to a certain amount of time being needed during the deformation of the silicon film and the flow of the internal liquid. When the loading frequencies further increased over 100 Hz (Figure 11b), the cyclic displacements were still visible. The bandwidth of the system can be analyzed more clearly in Figure 11c. With the increase in frequency, the variation range of displacement was not greatly attenuated, which proves that the SEHPA also had a good response to high-frequency voltage. In summary, the SEHPA can respond to the cyclic loading of 5 kV at 0~400 Hz. The vibrations of the SEHPA at different

frequencies are recorded in Video S2. It was also possible to generate vibration through pressure changes, as shown in Video S3, but we did not investigate this part further, because the SEHPA responded faster to electro-hydraulic drives.

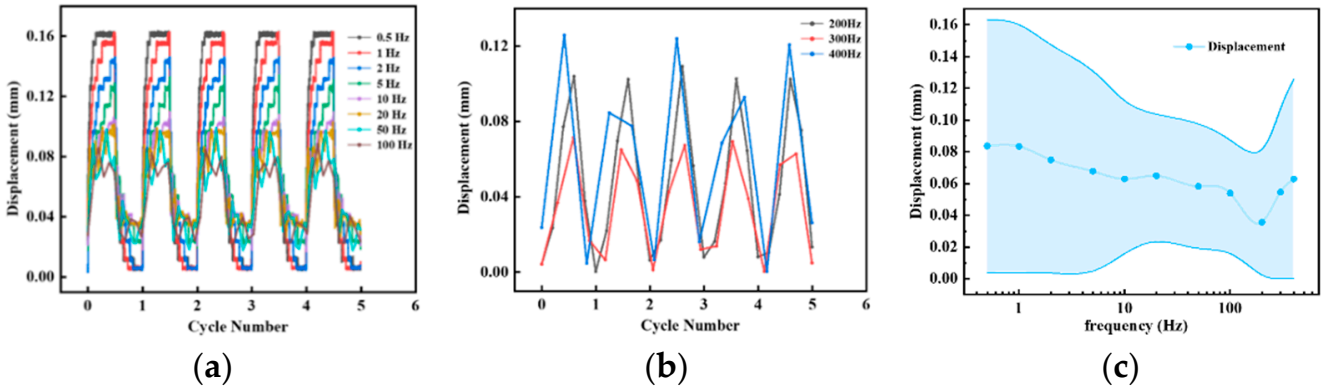

Figure 11. Displacements of SEHPA under the cyclic loading of 5 kV, with the loading frequencies of (**a**) 0~100 Hz and (**b**) 200~400 Hz. (**c**) The frequency response graph of the actuator displacement (mm) vs. actuation frequency (Hz). The loader pressure was 5 kPa.

4.2. Self-Sensing Closed-Loop Control of SEHPA

From the aforementioned results, the SEHPA exhibited self-sensing properties; namely, the current deformation state of the SEHPA could be analyzed with the resistance of the lower electrode. Therefore, a closed-loop control of the SEHPA was designed and is schematically described in Figure 12. The resistance value of the lower electrode was dedicated to matching with the corresponding tactile information, and the obtained resistance value was further input into the haptic feedback system. The system was adjusted by a PID control, and by comparing the set value of resistance with the actual value of resistance, the linear motor pushed the piston until the resistance value of the SEHPA reached a dynamic equilibrium.

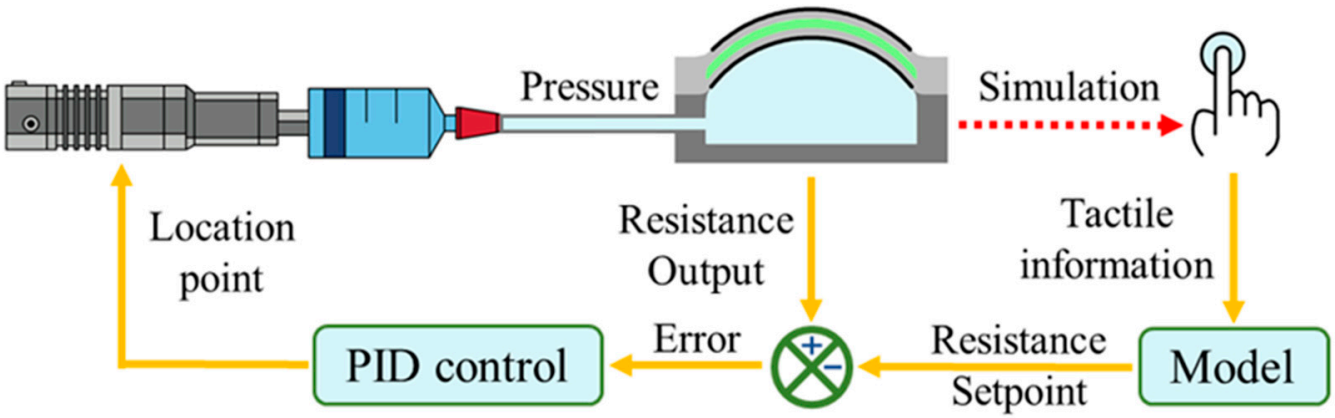

Figure 12. Closed-loop control flow chart of SEHPA.

The function between the lower electrode resistance and the output force of the SEHPA was obtained through experiments, as shown in Figure 13. The output force of the resistance in the dynamic equilibrium state was 70~110 kΩ. The curves could be divided into two stages, in which the output force increased sharply at 70~75 kΩ and the output force increased linearly and much more slowly at 75~110 kΩ. The two stages of the curves could be linearly fitted with the two following equations: $F = 0.11 \times R - 7.7$ $(70 < R < 75)$ and $F = 0.02833 \times R - 1.64893$ $(75 < R < 110)$. The input resistance value and output force value could therefore be converted through these two equations.

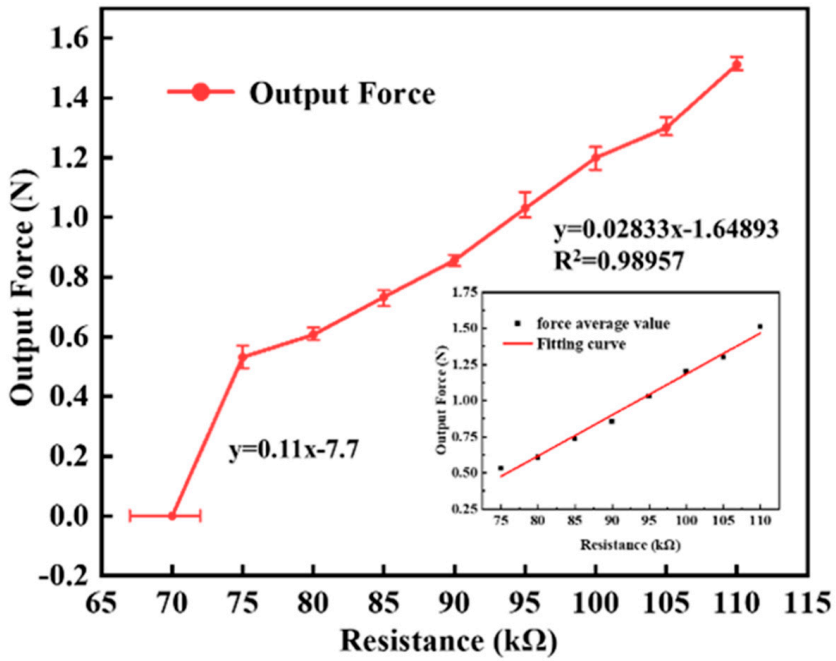

Figure 13. Relationship between lower electrode resistance versus output force of SEHPA under the closed-loop control system.

4.3. Application of SEHPA

4.3.1. Synchronous Haptic Feedback

The closed-loop control system (Figure 12) was used to accomplish the synchronous haptic feedback. An example to demonstrate the changes in resistance versus output force in the closed-loop control of the SEHPA is shown in Figure 14. With the aforementioned equation, a force of 1.2 N could be theoretically output with the input resistance of 100 kΩ. The dynamic equilibrium of the actual resistance of the electrode is the black line, and the corresponding output force, with a stable value of 1.2 N, is plotted as the orange line.

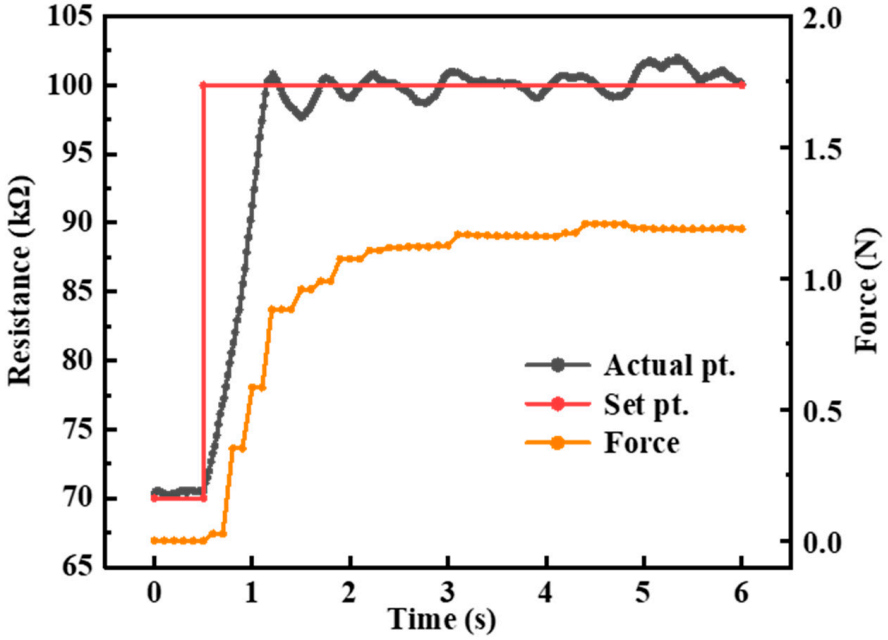

Figure 14. Demonstration of the closed-loop control of SHEPA, in which the set resistance was 100 kΩ.

In Video S4, the operator pressed the pressure sensor with their finger as the input of tactile information. The force information obtained through the pressure sensor would be matched with the resistance value information in Figure 13, and the corresponding resistance value would be input into the system as the set value. The red line on the screen is the real-time set value of the resistance, and the blue line is the resistance monitoring value. The resistance detection value can follow the set value, and the indicator of the dynamometer also changes correspondingly.

4.3.2. Application of Haptic Notifications

A mechanical gripper was used to simulate grasping a small ball with a human hand, while the tactile sensation was reproduced by the SEHPA. During the experiment, the mechanical gripper kept moving at a constant speed and was in contact with a small ball. The resistance signals, reflecting the magnitude of the loading force, collected by the pressure sensor (FSR402 RP-C18.3-LT, Interlink Electronics) on the gripper were converted into the corresponding input signal of the SEHPA. The SEHPA further deformed quickly to output nearly the same contact force as the mechanical gripper.

Three small balls with different hardness were grasped by a mechanical gripper with the same grasping force and grasping speed, in which the balls were a sponge ball, foam ball, and table tennis ball. The response of the SEHPA to grasp different balls is shown in Figure 15. The output displacements and the lower-electrode resistances of the SEHPA were different when grasping different balls. The difference in displacement of the SEHPA is not only related to the deformation of the hard ball, but also related to the pressure sensor installed in the mechanical gripper. In five cyclic grabs of the three balls, the actual resistance value of the SEHPA could fit with the input resistance value in real time, where the data acquisition interval was about 0.028 s.

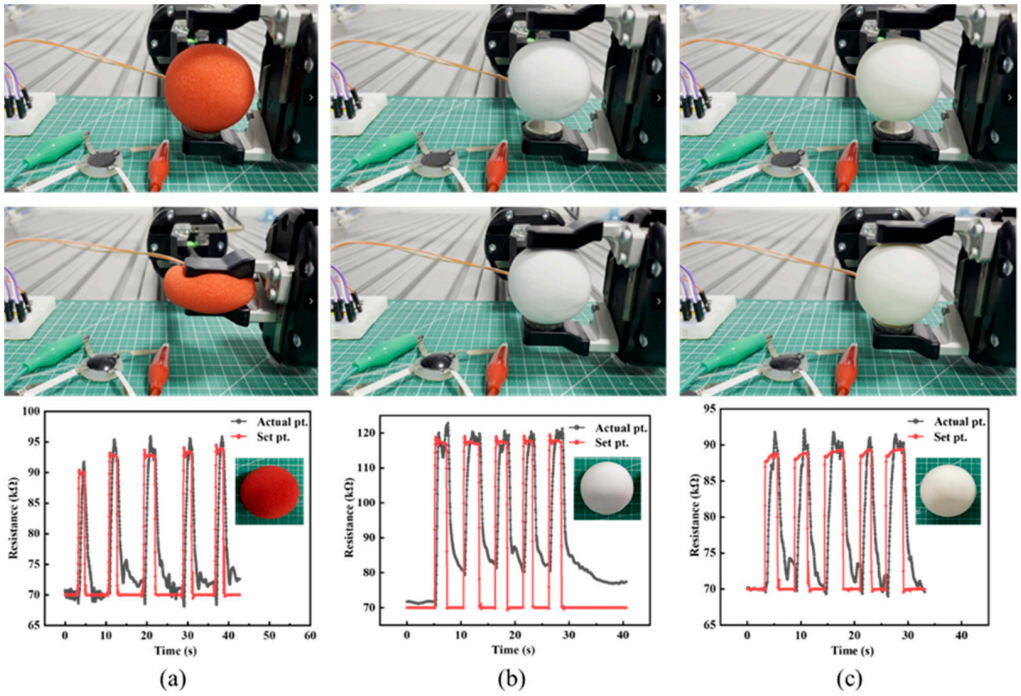

Figure 15. The response of SEHPA when balls with different hardness of (**a**) sponge ball, (**b**) foam ball, and (**c**) table tennis were clamped by a mechanical gripper.

From the above responses to the three balls, the resistance information, derived from Figure 16, can be dedicated to distinguishing the different balls with various hardness. Under the constant grasping speed and grasping force, a longer resistance rising time refers to a larger deformation of the ball, as well as a lower hardness of the ball. The difference in

the resistance stability value is related to the deformation of the ball and the characteristics of the pressure sensor itself. The too large or too small a deformation of the ball will lead to a low force value being obtained by the sensor. The results imply that the hardness information can be completely determined by the change in resistance with time (the time required for resistance to rise and reach stability). Herein, the different hardness of balls can be sensed and conveyed to hands with various vibration frequencies of the SEHPA, in which the vibration was produced by the electric hydraulic method. We therefore endow the three balls, the sponge ball, the foam ball, and the table tennis, with the vibrations of 2 Hz, 10 Hz, and 20 Hz, respectively. Accordingly, the objects with similar hardness to the three balls can hence be sensed with the setting vibration frequencies. Relevant content is displayed in Video S5. Similarly, other kinds of information cannot be sensed by primitive touch, such as the magnitude of forces, and can be defined and conveyed through the difference in vibrations. Video S6 shows the haptic notifications in the haptic feedback process, an alternative way to quickly convey defined information (for example, the exact magnitude of the force) without disrupting the overall haptic feedback process. Our work provides a new understanding in transmitting information that cannot be sensed by primitive touch, which will be beneficial to the fields of human–computer interaction and teleoperation.

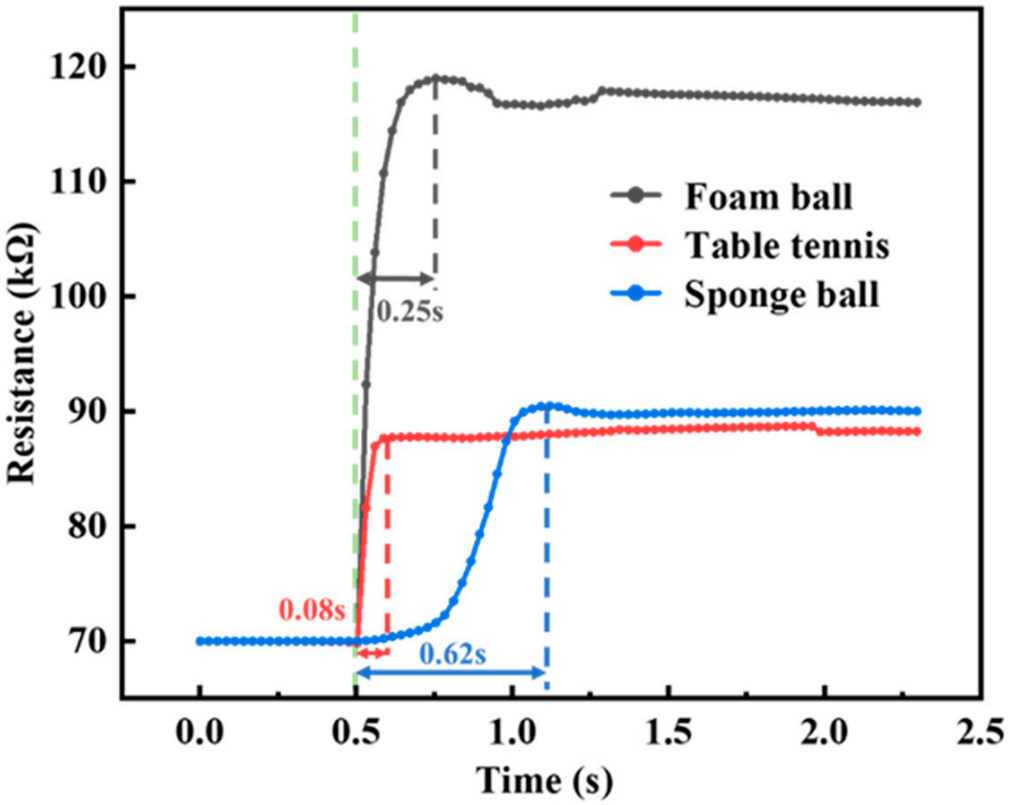

Figure 16. The resistance set value while grasping three kinds of balls.

5. Conclusions

We propose a novel way to generate haptic feedback by designing and manufacturing a SEHPA with the synergy of two driven modes of electro-hydraulic and pneumatic methods. The response characteristics, including output force, displacement, and resistance changes of the SEHPA, under pressures (0~10 kPa) and voltages (0~5 kV), were systematically characterized. The maximum output force and displacement of the SEHPA can reach 1.5 N and 4.5 mm. The electro-hydraulic drive can control the displacement and force transformation of the SEHPA in a small range (0~45 mN, 0~0.8 mm). As the human hand can distinguish about 0.2 g (20 mN) of weight change, the maximum increment in

45 mN produced by the electro-hydraulic drive is enough to be felt by the fingertips. This small force change can transmit other information without destroying the whole tactile feedback process. The closed-loop feedback system can be designed by using the self-sensing capability of the SEHPA and the output can be controlled more accurately by PID control. The combination of the two drives allows the SEHPA to maintain a high output and enough bandwidth to generate multi-modal vibration. During the experiment, the SEHPA, with its self-sensing capability, can smoothly simulate the tactile information in the whole operation. The SEHPA produces better tactile feedback in a variety of applications. The SEHPA can respond to voltages with various frequencies up to 400 Hz, thus generating vibrations of the same frequency. The practical application shows that the vibration hints of the SEHPA can convey the information of force and hardness, which cannot be perceived by human touch. A variety of tactile information can be conveyed using the SEHPA alone. Using the SEHPA, the easily imitated information can be imitated more accurately, and the difficultly imitated information can be replaced by vibration information, which is the application scheme in the field of tactile feedback. In the following research, we will study the miniaturization, densification, and integration control methods of the SEHPA, and remove the bonding of the cable, so as to further expand the application field of the SEHPA.

Supplementary Materials: The following supporting information can be downloaded at: https://www.mdpi.com/article/10.3390/act11030074/s1, Video S1: The output state of SEHPA at different pressures; Video S2: The different frequencies of vibrations by electro-hydraulic drive; Video S3: The vibration by pneumatic drive; Video S4: Synchronous haptic feedback by closed-loop control; Video S5: Haptic notifications (2 Hz, 10 Hz, and 20 Hz of vibration) to help the operator to distinguish the hardness of three different balls; Video S6: Haptic notifications transmit other information without interfering with the overall haptic feedback process.

Author Contributions: Conceptualization, H.W. and X.C.; methodology, H.W., X.C., P.H. and J.M.; software, M.Y. and S.P.; validation, H.W.; formal analysis, H.W.; investigation, H.W., X.C., J.M. and M.Y.; resources, X.C. and Y.C.; writing—original draft preparation, H.W. and P.H.; writing—review and editing, H.W., P.H. and X.C.; supervision, Z.J., P.W., Y.Y. and W.Y.; project administration, X.C., Z.J., P.W., Y.Y. and W.Y.; funding acquisition, Z.J. and X.C. All authors have read and agreed to the published version of the manuscript.

Funding: This research was funded by the National Natural Science Foundation of China (No. 51905530, 91748209), Beijing Nova Program of China (No. 2020B00003127), Zhuhai Industrial Core and Key Technology Research Project of China (No. ZH01084702180085HJL), and Programme 173.

Institutional Review Board Statement: Not applicable.

Informed Consent Statement: Not applicable.

Data Availability Statement: Data are contained within the article.

Conflicts of Interest: The authors declare no conflict of interest.

References

1. Yu, X.; Xie, Z.; Yu, Y.; Lee, J.; Vazquez-Guardado, A.; Luan, H.; Ruban, J.; Ning, X.; Akhtar, A.; Li, D.; et al. Skin-integrated wireless haptic interfaces for virtual and augmented reality. *Nature* **2019**, *575*, 473–479. [CrossRef] [PubMed]
2. Gallo, S.; Son, C.; Lee, H.J.; Bleuler, H.; Cho, I.-J. A flexible multimodal tactile display for delivering shape and material information. *Sens. Actuators A-Phys.* **2015**, *236*, 180–189. [CrossRef]
3. Kappassov, Z.; Corrales, J.-A.; Perdereau, V. Tactile sensing in dexterous robot hands-Review. *Robot. Auton. Syst.* **2015**, *74*, 195–220. [CrossRef]
4. Kim, Y.; Cha, J.; Ryu, J.; Oakley, I. A Tactile Glove Design and Authoring System for Immersive Multimedia. *IEEE Multimed.* **2009**, *17*, 34–44. [CrossRef]
5. Sarakoglou, I.; Garcia-Hernandez, N.; Tsagarakis, N.G.; Caldwell, D.G. A high performance tactile feedback display and its integration in teleoperation. *IEEE Trans. Haptics* **2012**, *5*, 252–263. [CrossRef]
6. Bianchi, M.; Battaglia, E.; Poggiani, M.; Ciotti, S.; Bicchi, A. A wearable fabric-based display for haptic multi-cue delivery. In Proceedings of the 24th IEEE Haptics Symposium, Philadelphia, PA, USA, 8–11 April 2016; pp. 277–283.
7. Gu, W.; Zhu, X.; Futai, N.; Cho, B.S.; Takayama, S. Computerized microfluidic cell culture using elastomeric channels and Braille displays. *Proc. Natl. Acad. Sci. USA* **2004**, *101*, 15861–15866. [CrossRef]

8. Lv, J.-A.; Liu, Y.; Wei, J.; Chen, E.; Qin, L.; Yu, Y. Photocontrol of fluid slugs in liquid crystal polymer microactuators. *Nature* **2016**, *537*, 179–184. [CrossRef] [PubMed]
9. Gorissen, B.; Reynaerts, D.; Konishi, S.; Yoshida, K.; Kim, J.-W.; Volder, M.D. Elastic inflatable actuators for soft robotic applications. *Adv. Mater.* **2017**, *29*, 1604977. [CrossRef] [PubMed]
10. Tang, S.-Y.; Zhang, X.; Sun, S.; Yuan, D.; Zhao, Q.; Yan, S.; Deng, L.; Yun, G.; Zhang, J.; Zhang, S.; et al. Versatile microfluidic platforms enabled by novel magnetorheological elastomer microactuators. *Adv. Funct. Mater.* **2018**, *28*, 1705484. [CrossRef]
11. Liu, Q.; Zhan, Y.; Wei, J.; Ji, W.; Hu, W.; Yu, Y. Dual-responsive deformation of a crosslinked liquid crystal polymer film with complex molecular alignment. *Soft Matter* **2017**, *13*, 6145–6151. [CrossRef]
12. Takagi, K.; Kitazaki, Y.; Kondo, K. A Simple Dynamic Characterization Method for Thin Stacked Dielectric Elastomer Actuators by Suspending a Weight in Air and Electrical Excitation. *Actuators* **2021**, *10*, 40. [CrossRef]
13. Rothemund, P.; Kellaris, N.; Mitchell, S.K.; Acome, E.; Keplinger, C. HASEL Artificial Muscles for a New Generation of Lifelike Robots-Recent Progress and Future Opportunities. *Adv. Mater.* **2021**, *33*, 2003375. [CrossRef] [PubMed]
14. Tang, W.; Lin, Y.; Zhang, C.; Liang, Y.; Wang, J.; Wang, W.; Ji, C.; Zhou, M.; Yang, H.; Zou, J. Self-contained soft electrofluidic actuators. *Sci. Adv.* **2021**, *7*, eabf8080. [CrossRef] [PubMed]
15. Lee, E.-H.; Kim, S.-H.; Yun, K.-S. Three-Axis Pneumatic Haptic Display for the Mechanical and Thermal Stimulation of a Human Finger Pad. *Actuators* **2021**, *10*, 60. [CrossRef]
16. Li, M.; Luo, S.; Nanayakkara, T.; Seneviratne, L.D.; Dasgupta, P.; Althoefer, K. Multi-fingered haptic palpation using pneumatic feedback actuators. *Sens. Actuators A Phys.* **2014**, *218*, 132–141. [CrossRef]
17. Song, K.; Kim, S.H.; Jin, S.; Kim, S.; Lee, S.; Kim, J.-S.; Park, J.-M.; Cha, Y. Pneumatic actuator and flexible piezoelectric sensor for soft virtual reality glove system. *Sci. Rep.* **2019**, *9*, 8988. [CrossRef]
18. Uramune, R.; Ishizuka, H.; Hiraki, T.; Kawahara, Y.; Ikeda, S.; Oshiro, O. HaPouch: Soft and Wearable Haptic Display Devices using Liquid-to-gas Phase Change Actuator. In Proceedings of the 33rd Annual ACM Symposium on User Interface Software and Technology, New York, NY, USA, 20–23 October 2020; pp. 53–55. [CrossRef]
19. Frediani, G.; Boys, H.; Ghilardi, M.; Poslad, S.; Busfield, J.J.C.; Carpi, F. A Soft Touch: Wearable Tactile Display of Softness Made of Electroactive Elastomers. *Adv. Mater. Technol.* **2021**, *6*, 16. [CrossRef]
20. Leroy, E.; Hinchet, R.; Shea, H. Multimode Hydraulically Amplified Electrostatic Actuators for Wearable Haptics. *Adv. Mater.* **2020**, *32*, 2002564. [CrossRef]
21. Koo, I.M.; Jung, K.; Koo, J.C.; Nam, J.-D.; Lee, Y.K.; Choi, H.R. Development of soft-actuator-based wearable tactile display. *IEEE Trans. Robot.* **2008**, *24*, 549–558. [CrossRef]
22. Chakraborti, P.; Karahan Toprakci, H.A.; Yang, P.; Di Spigna, N.; Franzon, P.; Ghosh, T. A compact dielectric elastomer tubular actuator for refreshable Braille displays. *Sens. Actuators A Phys.* **2012**, *179*, 151–157. [CrossRef]
23. Sonar, H.A.; Gerratt, A.P.; Lacour, S.P.; Paik, J. Closed-loop haptic feedback control using a self-sensing soft pneumatic actuator skin. *Soft Robot.* **2020**, *7*, 22–29. [CrossRef] [PubMed]
24. Joshi, S.; Sonar, H.; Paik, J. Flow path optimization for soft pneumatic actuators: Towards optimal performance and portability. *IEEE Robot. Autom. Lett.* **2021**, *6*, 7949–7956. [CrossRef]
25. Sparks, J.L.; Vavalle, N.A.; Kasting, K.E.; Long, B.; Tanaka, M.L.; Sanger, P.A.; Schnell, K.; Conner-Kerr, T.A. Use of Silicone Materials to Simulate Tissue Biomechanics as Related to Deep Tissue Injury. *Adv. Ski. Wound Care* **2015**, *28*, 59–68. [CrossRef] [PubMed]
26. Grushko, S.; Vysock, A.; Oscadal, P.; Vocetka, M.; Novak, P.; Bobovsky, Z. Improved Mutual Understanding for Human-Robot Collaboration: Combining Human-Aware Motion Planning with Haptic Feedback Devices for Communicating Planned Trajectory. *Sensors* **2021**, *21*, 3673. [CrossRef] [PubMed]
27. Acome, E.; Mitchell, S.K.; Morrissey, T.G.; Emmett, M.B.; Benjamin, C.; King, M.; Radakovitz, M.; Keplinger, C. Hydraulically amplified self-healing electrostatic actuators with muscle-like performance. *Science* **2018**, *359*, 61–65. [CrossRef]
28. Kellaris, N.; Venkata, V.G.; Rothemund, P.; Keplinger, C. An analytical model for the design of Peano-HASEL actuators with drastically improved performance. *Extrem. Mech. Lett.* **2019**, *29*, 100449. [CrossRef]
29. Guo, W.; Wang, X.; Lu, X.; Li, X.; Li, Y.; Sun, J. Plant oil and amino acid-derived elastomers with rapid room temperature self-healing ability. *J. Mater. Chem. A* **2019**, *7*, 21927–21933. [CrossRef]
30. Chang, W.; Kanda, H.; Ikeda, R.; Ling, J.; DeBerry, J.J.; Gu, J.G. Merkel disc is a serotonergic synapse in the epidermis for transmitting tactile signals in mammals. *Proc. Natl. Acad. Sci. USA* **2016**, *113*, E5491–E5500. [CrossRef]
31. Huang, P.; Cao, Y.; Wei, Y.; Cheng, X.; Liu, J.; Zhang, S.; Wang, P.; Chen, S.; Xia, Z. Anisotropic Printed Resistor with Linear Sensitivity Based on Nano–Microfiller-Filled Polymer Composite. *Adv. Electron. Mater.* **2021**, *7*, 2100581. [CrossRef]
32. Huang, P.; Xia, Z.; Cui, S. 3D printing of carbon fiber-filled conductive silicon rubber. *Mater. Des.* **2018**, *142*, 11–21. [CrossRef]